Suppression of the Critical Current and the Superfluid Transition Temperature of ³He in a Single Submicron Cylindrical Channel

J. P. Pekola, J. C. Davis, Zhu Yu-Qun,* R. N. R. Spohr,† P. B. Price, and R. E. Packard

Department of Physics, University of California, Berkeley, California

We report on an investigation into confined geometry effects and critical currents of superfluid ³He in a single circular cylindrical channel. The diameter of the channel, 0.7 μm, is of the order of the (temperature-dependent) coherence length and its aspect ratio is ~10. The reduction of the critical temperature demonstrates diffuse scattering on the solid walls of the microchannel. Using the Ginzburg–Landau formulation, we derive a model for the critical current and the critical temperature in a small, infinitely long, cylindrical channel with a circular cross section. The measured reductions of these quantities are in reasonable agreement with the predictions of the model.

1. INTRODUCTION

In the investigation of the properties of the three known quantum fluids (He II, ³He, and superconductors) the detailed structure of the order parameters is often not apparent when experiments are carried out on bulk or unbounded material. This is because the length scales for local variation of the order parameter are usually much smaller than the sample sizes used. Therefore, some of the most revealing experiments on superconductors have been carried out in restricted geometries.[1]

The object of this work is to study the effects of flow on superfluid ³He confined to a single cylindrical channel whose diameter is of the order of the (temperature-dependent) coherence length. This well-characterized restricted geometry allows knowledge to be gained about details of the spatial variation and form of the order parameter.

*Permanent address: University of Science and Technology, Wuhan, Hubei, China.
†Permanent address: Gesellschaft für Schwerionenforschung, Darmstadt, West Germany.

47

The outline of the paper is as follows: Section 2 introduces the main theoretical effects of the existence of channel boundaries on the order parameter and on various critical velocities. Section 3 discusses the depairing critical current in different geometries, with the main emphasis on our own model of the present problem. Section 4 gives details of the experiment and measurement techniques and discusses the primary data acquired, while Section 5 compares the relevant measured parameters with existing theoretical models. Section 6 is a brief summary of our conclusions.

2. CONFINED GEOMETRY EFFECTS AND CRITICAL FLOW

2.1. Order Parameter and Quasiparticle Scattering

The free energy functional of a superfluid state depends not only on the magnitude of the order parameter ψ, but also on its spatial variation. In the simplest s-wave superfluid the Ginzburg–Landau (GL) free energy density f is given by[2,3]

$$f = -\bar{\alpha}|\psi|^2 + \frac{\bar{\beta}}{2}|\psi|^4 + \frac{\hbar^2}{2M}|\nabla\psi|^2 \tag{1}$$

where $\bar{\alpha}$ and $\bar{\beta}$ are GL coefficients with known properties in the weak coupling limit and M is the mass of the condensed object (which for ^{3}He is $2m_3$). The last term $(\hbar^2/2M)|\nabla\psi|^2$ sets a lower limit for the length scale of spatial changes of ψ. This length $\xi \sim \hbar/(2M\bar{\alpha})^{1/2}$ is called the superfluid coherence length and it diverges near the superfluid transition temperature T_c as $(1 - T/T_c)^{-1/2}$.

In a p-wave superfluid such as ^{3}He the order parameter is given by a tensor $A_{\mu i}$ which has the dimensions of energy. Its components transform as a vector in spin space with respect to μ and as a vector in momentum space with respect to i.[3] A solid wall suppresses different components of $A_{\mu i}$ by amounts that are determined by the type of quasiparticle scattering at the wall.[4-7]

The two extreme boundary conditions are specular (or mirror) reflection and diffuse (or random) reflection. Numerical calculations on the behavior of the different components of the order parameter have been performed by solution of the gap equation in the GL region[4] and by quasiclassical Green's functions method.[5-7] The first approach reveals the boundary structure of the components at temperatures close to T_c, while the latter approach extends the study to all temperatures.

With the existence of a boundary we denote the components parallel to the wall as $A_{\mu\parallel}$ and the components perpendicular to it as $A_{\mu\perp}$. Specular scattering affects appreciably only the perpendicular component $A_{\mu\perp}$. The longitudinal components $A_{\mu\parallel}$ remain almost identical to the bulk value $A^0_{\mu i}$,

but the perpendicular component is suppressed to zero at a wall and heals to its bulk value over a distance several times $\xi(T)$. By contrast, in diffuse scattering all components are suppressed near the wall. The perpendicular component behaves as in the specular scattering case and, in addition, the longitudinal components are suppressed as well. At the wall $A_{\mu\parallel} < 0.5A^0_{\mu i}$ and heals in a length of about $\xi(T)$.

Physical effects of diffuse and specular boundary reflection on the superfluid state in a cylindrical channel have been studied by Barton and Moore[8] and Kjäldman et al.[9] Experimentally one can distinguish the correct scattering limit by, for example, observing the superfluid transition temperature in the channel. Specular reflection theories predict no depression of T_c, whereas diffuse reflection theories predict[8,9]

$$T_c^p / T_c = \exp\left[-\frac{3}{5} a^2 \left(\frac{\xi_0}{R}\right)^2 \right] \tag{2}$$

in the GL temperature region. T_c^p is the transition temperature in the pore, R is the channel radius, $a = 2.40$, and ξ_0 is the coherence length at $T = 0$. Numerical calculations of T_c^p / T_c versus ξ_0 / R have been performed by Kjäldman et al.[9] using the gap equations and extending to $T = 0$. Barton and Moore[8] studied the GL equations for a cylindrical channel and they predicted that phase transitions occur in such restricted geometries in the vicinity of T_c. These phase transitions have so far not been confirmed by experiment.

2.2. Critical Flow Effects

In the B phase of ³He at least two effects can set an upper limit to superfluid velocities. The competition between these depends on the geometry of the flow channel and the temperatures involved. The two relevant velocities are:

(a) The velocity characteristic of the intrinsic maximal current. This is called the depairing critical velocity v_c and it is of the order of Δ/p_F, where Δ is the energy gap $[\Delta \approx 1.76 k_B T_c (1 - T / T_c)^{1/2}]$ and p_F is the Fermi momentum of ³He at this pressure.

(b) The velocity for the creation of quantized vortices is given by $v_v \sim (\hbar/m_3 d) \ln(d/a)$. Here m_3 is the mass of the ³He atom, d is the characteristic channel size, and a is the size of the vortex core.

We wish to study depairing effects in this experiment. Therefore it is necessary to suppress vortex creation in the channel. Since v_v depends strongly on channel size, one can choose the geometry such that vortex creation is unfavorable at all velocities up to the depairing critical velocity v_c. The channel diameter at which $v_v = v_c$ is seen in Fig. 1 to be $d \approx 2\ \mu$m. In our apparatus $d = 0.7\ \mu$m, well below the crossover diameter d_c. The
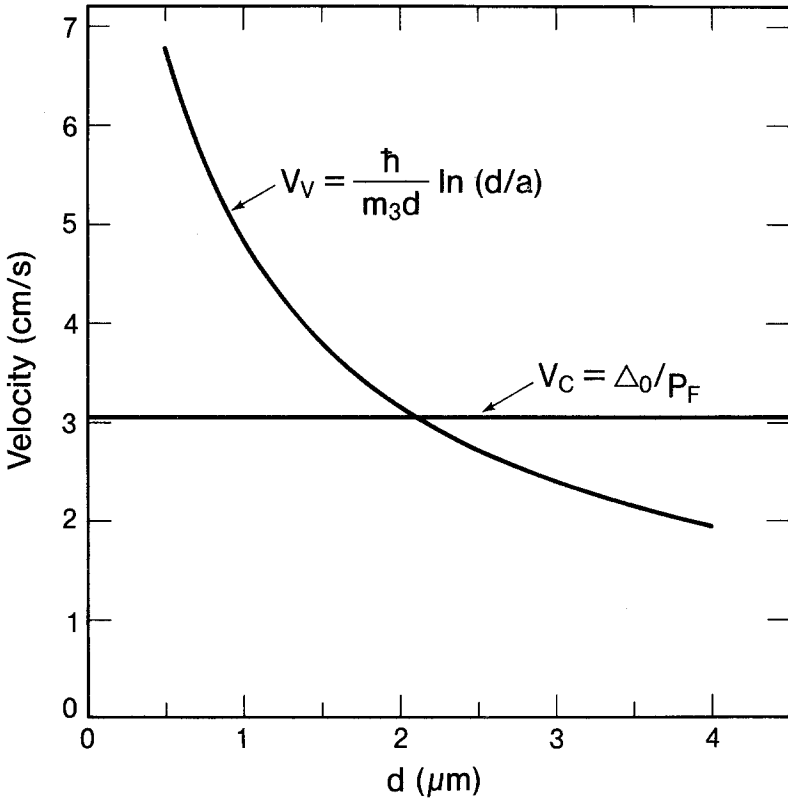
Fig. 1. The velocity for creation of single quantized vortex rings $v_v \sim (\hbar/m_3 d)\ln(d/a)$ (with $a = 0.1~\mu$m) and the depairing critical velocity $v_c \sim \Delta_0/p_F$ as a function of channel diameter. Δ_0 is the B-phase energy gap at $P = 0$ and $T = 0$.

condition $d < d_c$ for a long cylindrical ^{3}He channel makes this experimental arrangement an analogue of a 1d superconducting microbridge.[1]

3. DEPAIRING J_c IN UNBOUNDED AND RESTRICTED GEOMETRIES

In this section we discuss the intrinsic maximal supercurrent J_c, often called the depairing critical current.

In the absence of flow and in unbounded B phase the order parameter can be expressed as[3]

$$A = \Delta \begin{pmatrix} 1 & & \\ & 1 & \\ & & 1 \end{pmatrix} e^{i\phi} \tag{3}$$

if one neglects the rotation of spin components with respect to spatial components due to the small dipolar coupling energy. Here Δ is the (spherical) energy gap of the B phase: $\Delta^2 = \alpha/10\beta$, where

$$\alpha = \tfrac{1}{3}N(0)(1 - T/T_c)$$

$$\beta = [7\zeta(3)/240\pi^2]N(0)(k_B T_c)^{-2}$$

with $N(0)$ the density of states of one spin projection at the Fermi surface, $\zeta(3)$ the Riemann zeta function, and ϕ the overall phase of the order parameter.

The presence of flow distorts the energy gap, giving it a nonspherical form. The component of A parallel to the flow is reduced, yielding[10,11]

$$A = \Delta \begin{pmatrix} a & & \\ & a & \\ & & c \end{pmatrix} e^{iqz} \tag{4}$$

This represents uniform flow in the z direction with a superfluid velocity $v_s = (\hbar/2m_3)q$. Using this form for A, one finds the maximal mass current density J_c to be (in GL theory)[10-12]

$$J_c = \frac{8\pi\sqrt{5}}{9[7\zeta(3)]^{1/2}} \frac{\rho k_B T_c}{p_F} \left(1 - \frac{T}{T_c}\right)^{3/2} \tag{5}$$

Here ρ is the density of liquid ^{3}He. This calculation has been extended to all temperatures by Vollhardt et al.[10] and Kleinert.[11]

Jacobsen and Smith[13] have calculated J_c in the vicinity of the transition temperature for a one-dimensional polar phase. Their prediction is that the temperature-independent prefactor of the critical current is reduced to about one-half of its bulk value. Monien and Tewordt[14] have studied for the case of specular boundary scattering the current–phase characteristic of a short channel with rectangular cross section.

We introduce here a variational approach that is not rigorous, but produces confined-geometry effects at least semiquantitatively.

The model we choose presents A in cylindrical polar coordinates in the form

$$A = \begin{pmatrix} a & & \\ & a & \\ & & c \end{pmatrix} f(r) e^{iqz} \tag{6}$$

Here the flow axis, the channel axis, and the z axis coincide. The reasons for the choice of Eq. (6) are the following: For bulk fluid, A is of the form given by Eq. (4) and since we assume perfect cylindrical symmetry and no

vorticity in the channel, the effects of the walls on A will depend only on the radial variable r. We choose all the components to have the same radial variation, namely

$$f(r) = 1 - \exp[(r - R)/\xi(T)] \tag{7}$$

This form simulates diffuse reflection at the wall $r = R$, where R is the radius of the channel. Setting the r and ϕ components of A equal in Eq. (6) is not rigorous, but this choice avoids mathematical complications in the form of the resulting free energy that require the existence of singularities along the central axis of the flow channel.

For this model the relevant free energy density contains the condensation free energy density f_0 and the kinetic/bending free energy density f_K: $\mathscr{F} = f_0 + f_k$.

Buchholtz and Fetter[15] show the general expression for f_0 and f_k in cylindrical polar coordinates. For the order parameter of Eq. (6) one obtains from these equations in the weak coupling limit

$$f_0 = -\alpha(2a^2 + c^2)f^2 + \beta(8a^4 + 3c^4 + 4a^2c^2)f^4 \tag{8}$$

and

$$f_k = K(4a^2f'^2 + c^2f'^2 + 2a^2f^2q^2 + 3c^2f^2q^2) \tag{9}$$

Here $K = N(0)\xi_0^2/5$ and $f'(r) \equiv df(r)/dr$. The components a and c are taken to be real, since one can readily see from the original free energy expansion[15] that the phases of these two components are equal if $\mathscr{F}$ is minimized. Minimizing the average free energy per unit volume $\langle \mathscr{F} \rangle = \sigma^{-1} \int_\sigma dA \, \mathscr{F}$, where σ is the cross-sectional area of the channel, yields

$$a^2 = \frac{1}{10} \frac{\alpha\langle f^2 \rangle}{\beta\langle f^4 \rangle} - \frac{1}{4} \frac{K\langle f'^2 \rangle}{\beta\langle f^4 \rangle} \tag{10}$$

and

$$c^2 = \frac{1}{10} \frac{\alpha\langle f^2 \rangle}{\beta\langle f^4 \rangle} - \frac{1}{2} \frac{K\langle f^2 \rangle}{\beta\langle f^4 \rangle} q^2 \tag{11}$$

Thus, only the longitudinal component is explicitly affected by the superflow. From Eq. (10), $a^2 = 0$ at a temperature T_1 that depends on R. At temperatures above this the minimization of the average free energy per unit volume with $a^2 = 0$ yields

$$c^2 = \frac{\alpha\langle f^2 \rangle - K\langle f'^2 \rangle - 3\langle f^2 \rangle Kq^2}{6\beta\langle f^4 \rangle} \tag{12}$$

T_1 represents a transition temperature above which the liquid is in a polar phase. (For our experimental arrangement $T_1/T_c \approx 0.6$ at $P = 0$ and $T_1/T_c \approx 0.7$ at $P = 2.4$ bar.)

The superfluid mass current density in the z direction is given by

$$J_z = (4m_3 K / \hbar)(2a^2 + 3c^2)f^2 q \tag{13}$$

according to the general expression for J_z in cylindrical polar coordinates. Substituting a^2 and c^2 from Eqs. (10) and (11), or from (12) when $a^2 = 0$, yields

$$J_z = \frac{2m_3 K \langle f^2 \rangle}{\hbar} \left[\left(\frac{\alpha \langle f^2 \rangle}{\beta \langle f^4 \rangle} - \frac{K \langle f'^2 \rangle}{\beta \langle f^4 \rangle} \right) q - \frac{3K \langle f^2 \rangle}{\beta \langle f^4 \rangle} q^3 \right] \tag{14}$$

This has a maximum value

$$J_c^p = \frac{4}{9} \frac{m_3 K \langle f^2 \rangle}{\hbar} \frac{(\alpha \langle f^2 \rangle - K \langle f'^2 \rangle)^{3/2}}{(K \langle f^2 \rangle)^{1/2} \beta \langle f^4 \rangle} \tag{15}$$

which occurs at $q = q_c$, where

$$q_c = \left[\frac{\alpha \langle f^2 \rangle - K \langle f'^2 \rangle}{9K \langle f^2 \rangle} \right]^{1/2} \tag{16}$$

In the unbounded liquid $\langle f^2 \rangle = \langle f^4 \rangle = 1$ and $\langle f'^2 \rangle = 0$, thus giving the bulk critical current J_c. Scaling the critical current in the channel J_c^p by the bulk critical current J_c yields, after evaluation of the averages using f from Eq. (7),

$$\frac{J_c^p}{J_c} = [1 - \tfrac{18}{5}u^{-1} + (\tfrac{19}{5} - 4e^{-u} - \tfrac{4}{5}e^{-2u})u^{-2}]^{3/2}$$

$$\times [1 - 3u^{-1} + (\tfrac{7}{2} - 4e^{-u} - \tfrac{1}{2}e^{-2u})u^{-2}]^{1/2}$$

$$\times [1 - \tfrac{25}{6}u^{-1} + (\tfrac{415}{72} - 8e^{-u} + 3e^{-2u} - \tfrac{8}{9}e^{-3u} + \tfrac{1}{8}e^{-4u})u^{-2}]^{-1} \tag{17}$$

Here $u = (R/\xi_0)(1 - T/T_c)^{1/2}$. From Eq. (17) one finds that J_c and c^2 vanish where $u^{-1} = 0.513$. This means that the critical temperature in the pore T_c^p is reduced from the bulk critical temperature by the amount

$$T_c^p / T_c = 1 - \left(\frac{\xi_0/R}{\gamma} \right)^2 \tag{18}$$

where $\gamma = 0.513$. Taking the first term in the Taylor series in Eq. (2) yields

$$\frac{T_c^p}{T_c} = 1 - \left(\frac{\xi_0/R}{0.537} \right)^2 \tag{19}$$

in close agreement with our estimate.

Below T_c^p, J_c^p depends on temperature in this model approximately as $(1 - T/T_c^p)^{3/2}$. Dividing through by $J_c/(1 - T/T_c)^{3/2}$ as given in Eq. (5) gives the reduction factor j, where

$$j = J_c^p(T = 0)/J_c(T = 0) \tag{20}$$

which is shown in Fig. 2 together with T_c^p/T_c as a function of ξ_0/R. Predicted values of T_c^p/T_c and j are the central results of our model.
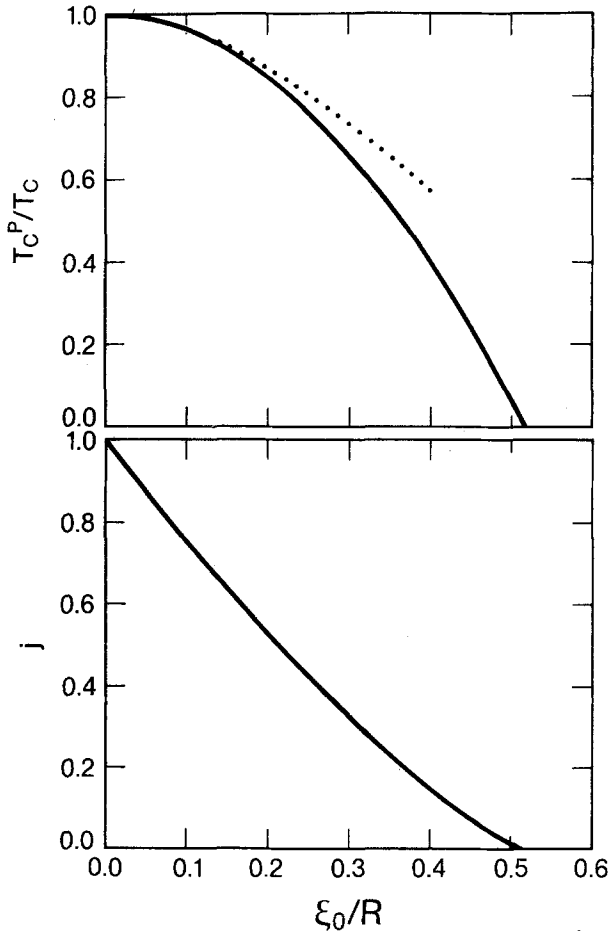

Fig. 2. The reduction of the critical temperature inside the channel from ($\cdots$) Eq. (2) and (—) our model, and the reduction of the critical current $j = J_c^p(T = 0)/J_c(T = 0)$ as a function of ξ_0/R, where R is the channel radius.

4. EXPERIMENTAL

4.1. Refrigeration

A conventional mK cryostat using a commercial dilution unit (SHE-DRP36) and a demagnetization stage made of a solid bar of copper is employed. Due to high base temperatures of the mixing chamber (20–26 mK) and an anomalous heat capacity at the lowest temperatures, the ^{3}He sample had a minimum temperature of 0.7 mK. After a few weeks' running, the ambient heat leak on the copper stage was $\dot{Q} \approx 1$ nW. These conditions allowed 3–6 h of measurement below 0.9 mK ($= T_c^p$ at $P = 0$) in each demagnetization cycle. At $P = 2.4$ bar the effective measurement time was 12–24 h.

4.2. Etched Nuclear Track Channel Production

We have described the technique of producing single channels in plastic diaphragms in detail elsewhere.[16]

A polycarbonate foil with thickness 6 μm is exposed to a single fission fragment from a ^{252}Cf source. This penetrating fragment produced a so-called latent track in the foil, which acts as a preferred target for etching by NaOH. By choosing the etch time, one can reproducibly fabricate in this material quite circular cylindrical channels with diameters from 0.3 to 10 μm. Examination of the channel using a scanning electron microscope reveals a surface roughness inside the channel that is no more than 10% of the radius.

We calibrate the etch rate of nuclear tracks using electron microscopy (TEM and SEM) and gas flow experiments. The single channel we employed was intended to have a diameter of 0.8 μm. The ^{4}He gas flow measurements at 77 K and liquid ^{3}He flow measurements at 1 K indicated a diameter of 0.7 μm. Much of our further analysis is based on this number.

4.3. Experimental Chamber

Figure 3 shows the essential features of the ^{3}He chamber. It has two approximately equal compartments separated by a flexible electrode made from a 10-μm polycarbonate foil. A 1000-Å gold layer is deposited on both sides. The lower metallic face is grounded and the upper one is electrically isolated. On both sides of this diaphragm are rigid electrodes at a distance of about 20 μm.

The 6-μm foil containing the flow channel is mounted using an indium O-ring such that it can be replaced by another without damage to the cell. The absence of parallel internal leaks is verified by replacing the flow channel holder by a solid brass piece. A mass spectrometer-based ^{4}He leak detector is connected to one compartment while admitting ^{4}He gas to the
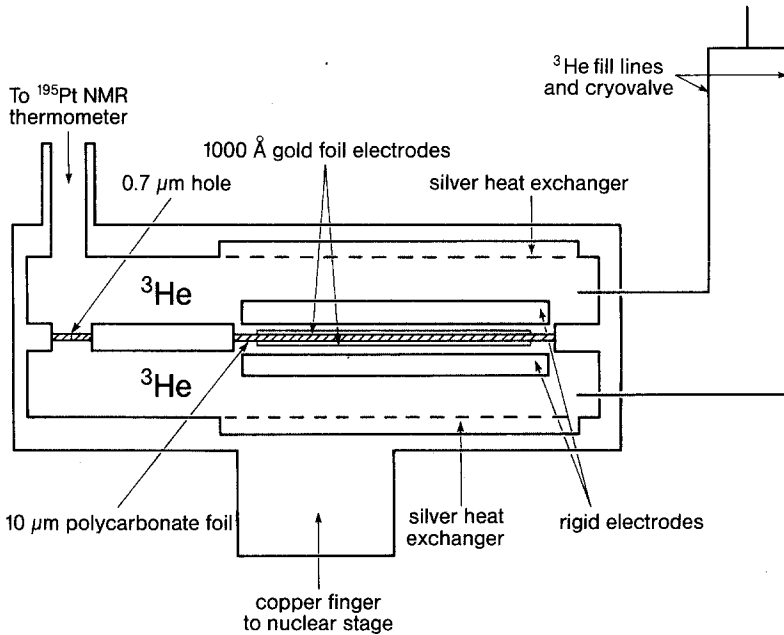
Fig. 3. A diagram of the experimental chamber used for the superflow measurements.

other. This test is carried out at 77 K. Absence of a ^{4}He signal at the detector indicates absence of a parallel flow path.

Both compartments have silver powder heat exchangers of surface area of 50 m^2 (approx.) to maintain thermal equilibrium with the cooper cooling stage. Nuclear susceptibility of platinum powder in the liquid ^{3}He is used for thermometry. The thermometer calibration constant is determined at the bulk transition temperature T_c, which was detected both by a change of the heat capacity of the ^{3}He sample and as a (characteristic) anomaly in the capacitance of the position sensor while cooling or warming through T_c (see Fig. 4).

The ^{3}He was admitted to the cell through two separate fill lines. To study flow through the microchannel, it was necessary to remove the parallel flow path through these fill lines. Two methods were used to do this.

(a) In early runs the fill lines were isolated from the cell using two mechanical needle valves mounted on the 1 K plate.

(b) In later runs the two halves of the cell were interconnected with a long, thin capillary of diameter 100 μm and length 3 m. This had a very high flow impedance at lowest temperatures because of the high normal fluid viscosity of ^{3}He, $\eta = (0.2/T^2)$ kg mK^2/msec. The resulting flow time constant through this parallel path was 2–5 h which means that the amount
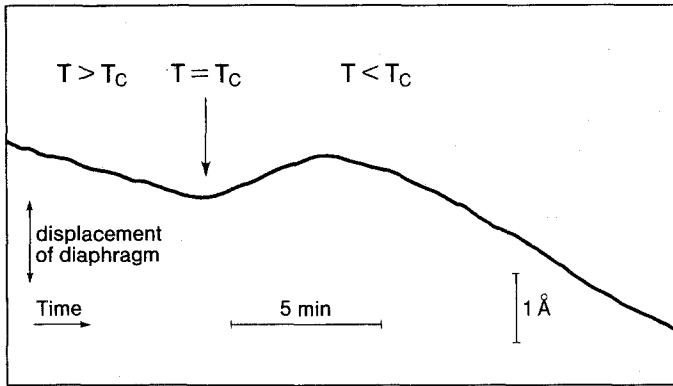
Fig. 4. The position of the measurement diaphragm as a function of time as T passes through T_c. This characteristic feature provides the calibration point for the thermometry (see text).

of parallel normal mass current during measurements of superflow is negligible.

The cryovalve permitted measurements with no parallel flow path, but its location at the 1 K plate caused serious noise problems in the cell. The two fill lines, running separately below the closed valve, feel temperature variations in different parts of the refrigerator. This results in pressure fluctuations at the cell.

The high-impedance interconnection method had the advantage that at the saturated vapor pressure it is possible to have the free surface of ^{3}He just above the interconnection point and inside a 2-cm^3 ballast volume at the mixing chamber. This method reduced the noise level by a factor of 300 relative to the double cryovalve system. The final noise level of the displacement transducer is 8×10^{-12} m/Hz$^{1/2}$. Expressed as a pressure noise, this is 1.6×10^{-4} Pa/Hz$^{1/2}$.

4.4. Measurement Techniques

The capacitance C between the rigid metal electrode in the top half of the cell and the electrically isolated top side of the diaphragm is the basic parameter measured in the experiment. The rate of change of C ($= \dot{C}$) is proportional to the current J_s through the channel, and the deviation of C from its equilibrium value (ΔC) is proportional to the instantaneous pressure drive ΔP across the channel. The lower capacitor formed by the rigid electrode in the bottom half of the cell and the lower side of the diaphragm can be biased at some voltage U, thus providing the drive to induce J_s and ΔP. The capacitance is measured using a bridge consisting

of a frequency synthesizer, an isolation transformer, a low-temperature (1 K) silver–mica capacitor (470 pF), a preamplifier, and a vector lock-in amplifier. The bridge excitation voltage was 100 mV p-p at 5 kHz and the lock-in time constant was 1 sec.

The dynamics of the experiment are described by two equations. One is the instantaneous balance equation for the position of the diaphragm, which equates the drive force per unit area to the sum of the elastic restoring force per unit area of the diaphragm and the pressure drop across the channel, i.e.,

$$g_0 U^2 = \Delta P + \lambda x \tag{21}$$

Here g_0 is a constant of the drive capacitor, U is the applied voltage, x is the spatial average displacement of the position-sensing diaphragm, and λ is its restoring constant in units of pressure per unit displacement. The numerical values for our apparatus are $g_0 = 9 \times 10^{-4}$ Pa/V^2 and $\lambda = 2 \times 10^7$ Pa/m.

The second equation governing the position of the diaphragm is obtained from mass conservation,

$$\sigma J_s = \rho A_m \dot{X} - \kappa \rho V \Delta \dot{P} \tag{22}$$

The left-hand side is the mass flux through the channel. The first term on the right is the mass displaced by a moving diaphragm of area A_m, where ρ is the mass density of the fluid. The second term on the right (which in our case is about 2% of the first) accounts for the compression/decompression of the liquid. Here κ is the compressibility of liquid ^{3}He, and V is the reduced volume of the container, $V^{-1} = V_1^{-1} + V_2^{-1}$, where V_1 and V_2 are the volumes of the compartments. Equations (21) and (22) are used to extract the relevant quantities J_s and ΔP from the primary data.

4.5. Primary Data

Toward the end of the demagnetization cycles one observes the transition into the superfluid state as is shown in Fig. 4. The drift in the baseline both above and below T_c is caused by the increase of the flow impedance of the two capillaries and the resulting unequal flow through them as a response to the small pressure changes at the top of the ^{3}He column. Due to this impedance mismatch, the balance of the capacitor is lost and is regained only when the temperature falls below T_c^p, because here the pressure could be quickly equilibrated by superflow through the microchannel. An example of this process is shown in Fig. 5.

Once the equilibrium is established, the apparatus is ready for measurement. The fluid is driven through the channel by applying a stepwise voltage of variable magnitude (between 0.8 and 5.0 V) to the drive capacitor. This
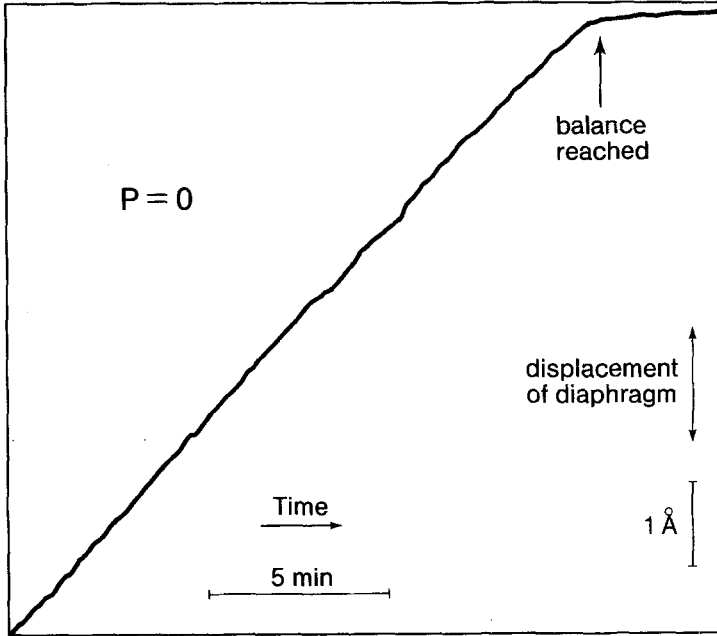
Fig. 5. The position of the measurement diaphragm as superflow through the channel equilibrates the initial pressure difference between the two volumes when the temperature first falls below T_c^p. When the two sides are at the same pressure the flow stops abruptly.

causes the capacitance measured at the upper capacitor to change at a rate proportional to J_s. Examples of primary data are shown in Fig. 6. A typical experimental run consists of measurements of J_s with different ΔP and at different temperatures T/T_c.

5. CRITICAL CURRENT AND CRITICAL TEMPERATURE

Measurements of $\dot{C}$ versus U^2 show that $\dot{C}$ essentially saturates with drive pressure above 10 mPa. This saturation of $\dot{C}$ is taken to represent the critical current. The initial onset of dissipation, i.e., the flow characteristics when $\Delta P < 10$ mPa, will be discussed in a separate paper.[17] Two runs, one at $P = 0$ and the other at $P = 2.4$ bar, are shown in Fig. 7.

The first obvious feature of the data in this figure is that they show that the measured maximum current falls to zero at a temperature much below the bulk transition temperature T_c. This depression of T_c in the pore is in close agreement with that predicted with our model for diffuse quasiparticle scattering at the walls.[9] It also agrees well with our model, which is represented by the solid line in Fig. 7.
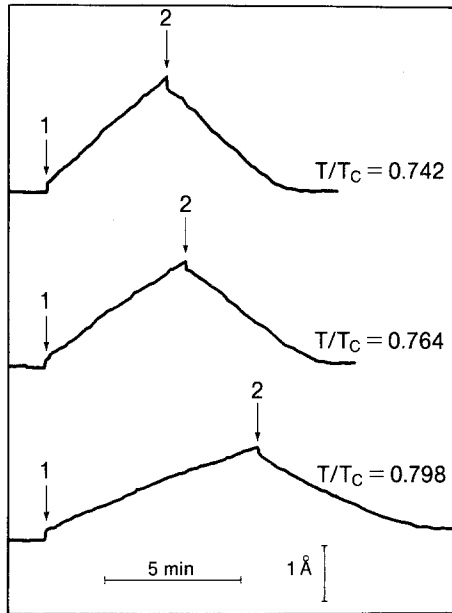
Fig. 6. Flow transients at various temperatures. Initially the capacitor is in balance and there is no flow. At point 1 a voltage of 4.1 V is applied to the drive side of the diaphragm. This is equivalent to a pressure $\Delta P = 14$ mPa. First there is a small compressional jump in the diaphragm position and then superflow begins to equilibrate the pressure head with a current proportional to the time rate of change of the diaphragm position. This current is independent of ΔP in this region of large ΔP. At point 2, when the pressure head has relaxed by only a few mPa, the voltage is turned off and the equilibrium position of the diaphragm returns to its original one. Superflow now equilibrates the few mPa built up initially, but in this small-ΔP region the current clearly depends on ΔP, as seen by "rounding" of the trace. This will be discussed in a separate paper.[17] The critical current is also seen to decrease with temperature. ΔP at any point in the falling traces is proportional to the vertical distance from the equilibrium line.
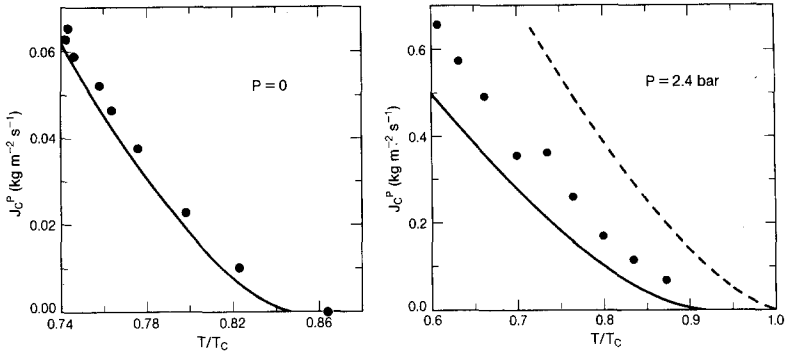
Fig. 7. (a) The critical current in the channel J_c^p as a function of T/T_c at $P = 0$ from (—) our model and (●) the data. The critical current predicted by considering only unbounded fluid is of-scale (at $T/T_c = 0.86$, $J_c = 0.16$ kg m^{-2} sec^{-1}). The systematic error in the temperature scale is 0.03 mK at most, and $T_c = 1.04$ mK. (b) The critical current in the channel as a function of T/T_c at $P \approx 2.4$ bar from (—) our model and (●) the data, and (- -) from theory considering only unbounded fluid. The systematic error of the temperature scale is 0.03 mK at most, and $T_c = 1.39$ mK.

The second important feature of the data in Fig. 7 is that the magnitude of the critical current is much reduced from that predicted for bulk liquid.[10-12] Here again the agreement between the measured J_c^p and that predicted by our variational estimate is good, as seen in the figure. At both pressures where measurements were taken the absolute reduction of the critical current is quite large.

At $P = 0$ the temperature dependence is somewhat uncertain due to the restricted range of temperatures reached. The best fit is obtained with the temperature dependence $(1 - T/T_c^p)^n$, with $n = 1.2$. At $P = 2.4$ bar the

TABLE I

Results of Measurements and Calculations of T_c^p/T_c, Current Reduction j, and the Exponent n of the Temperature Dependence of J_c^p at pressures 0 and 2.4 bar[a]

| P, bar | ξ_0/R | T_c^p/T_c | | | j | | n | |
		Measured	Present model	GL[8,9]	Measured[b]	Present model[c]	Measured	GL[10-12]
0	0.20	0.87	0.85	0.87	0.46	0.53	1.2	1.5
2.4	0.15	0.94	0.92	0.93	0.70	0.63	1.5	1.5

[a]The zero-temperature coherence length ξ_0 is from the specific heat measurements of ref. 20.
[b]From the best fit of the form $J_c^p = jJ_c(0)(1 - T_c/T_c^p)^{1.5}$, where, $J_c(0) = \{8\pi 5^{1/2}/9[7\zeta(3)]^{1/2}\}\rho k_B T_c/p_F$.
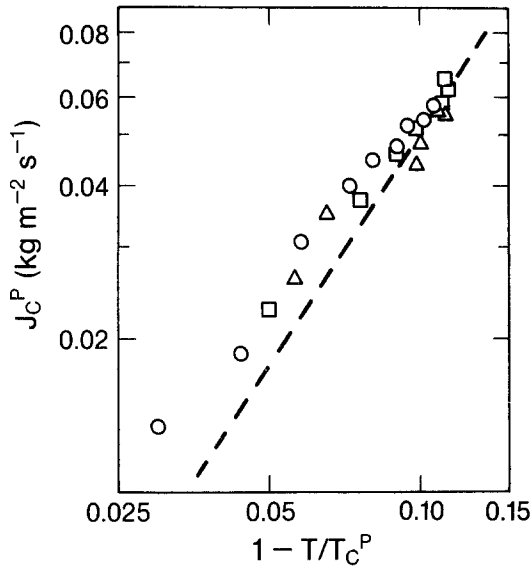[c]$j = J_c^p(T = 0)/J_c(T = 0)$.

Fig. 8. The critical current as a function of $(1 - T/T_c^p)$ from three different runs at $P = 0$. (--) From our model.

best fit to the data is obtained with temperature dependence $(1 - T/T_c^p)^n$, where $n = 1.5 \pm 0.2$. Three runs at $P = 0$ are shown in Fig. 8, plotted on a double logarithmic scale. Comparison of our experimental values of the parameters T_c^p, j, and the exponent n with their predicted values is presented in Table I.

6. CONCLUSIONS

The observed large suppression of the transition temperature in the channel T_c^p / T_c is a definite verification of diffuse scattering of quasiparticles at the walls of the microchannel. This has also been suggested by some earlier measurements on packed powders and random arrays of multiple micropores.[18,19] The measured suppression of the magnitude of the supercurrent clearly indicates diffuse scattering also and since the results of our own Ginzburg–Landau calculation closely agree with the observed effects of confined geometry on superflow, our choice of order parameter seems to be a reasonably good approximation. Our calculation suggests that the stable state of ^{3}He inside the narrow channel is a polar phase under our experimental conditions except at the lowest temperatures when $P = 2.4$ bar.

ACKNOWLEDGMENTS

REFERENCES

1. P. E. Lindelof, *Rep. Prog. Phys.* **44**, 949 (1981).
2. V. L. Ginzburg and L. D. Landau, *Zh. Eksp. Teor. Fiz.* **20**, 1064 (1950).
3. D. M. Lee and R. C. Richardson, in *The Physics of Liquid and Solid Helium, Part II*, K. H. Bennemann and J. B. Ketterson, eds. (Wiley, New York, 1978), p. 287.
4. V. Ambegaokar, P. G. deGennes, and D. Rainer, *Phys. Rev. A* **9**, 2676 (1974).
5. L. J. Buchholtz and D. Rainer, *Z. Physik B* **35**, 151 (1979).
6. Weiyi Zhang, J. Kurkijärvi, and E. V. Thuneberg, *Phys. Lett.* **109A**, 238 (1985).
7. L. J. Buchholtz, *Phys. Rev. B* **33**, 1579 (1986).
8. G. Barton and M. A. Moore, *J. Low Temp. Phys.* **21**, 489 (1975).
9. L. H. Kjäldman, J. Kurkijärvi, and D. Rainer, *J. Low Temp. Phys.* **33**, 577 (1978).
10. D. Vollhardt, K. Maki, and N. Schopohl, *J. Low Temp. Phys.* **39**, 79 (1980).
11. H. Kleinert, *J. Low Temp. Phys.* **39**, 451 (1980).
12. A. L. Fetter, in *Quantum Statistics and the Many Body Problem*, S. B. Trickey, W. P. Kirk, and J. W. Duffy, eds. (Plenum Press, New York, 1975), p. 127.
13. K. W. Jacobsen and H. Smith, personal communication; *J. Low Temp. Phys.* **67**, 83 (1987).
14. H. Monien and L. Tewordt, *J. Low Temp. Phys.* **62**, 277 (1986).
15. L. J. Buchholtz and A. L. Fetter, *Phys. Rev. B* **15**, 5225 (1977).
16. R. E. Packard, J. P. Pekola, P. B. Price, R. N. R. Spohr, K. H. Westmacott, and Zhu Yu-Qun, *Rev. Sci. Instr.* **57**, 1654 (1986).
17. J. P. Pekola, J. C. Davis, and R. E. Packard, to be published.
18. T. Chainer, Y. Morii, and H. Kojima, *J. Low Temp. Phys.* **55**, 353 (1984).
19. M. T. Manninen and J. P. Pekola, *Phys. Rev. Lett.* **48**, 812 (1982); **48**, 1369 (E) (1982); *J. Low Temp. Phys.* **52**, 497 (1983).
20. T. A. Alvesalo, T. Haavasoja, and M. T. Manninen, *J. Low Temp. Phys.* **45**, 373 (1981); T. Haavasoja, Ph.D. Thesis, Helsinki University of Technology (1980) unpublished.